Journal of Marine Research, 61, 465–489, 2003

Upper ocean control on the solubility pump of CO_2

by Takamitsu Ito[1] and Michael J. Follows[1]

ABSTRACT

We develop and test a theory for the relationship of atmospheric pCO_2 and the solubility pump of CO_2 in an abiotic ocean. The solubility pump depends on the hydrographic structure of the ocean and the degree of saturation of the waters. The depth of thermocline sets the relative volume of warm and cold waters, which sets the mean solubility of CO_2 in the ocean. The degree of saturation depends on the surface residence time of the waters.

We develop a theory describing how atmospheric CO_2 varies with diapycnal diffusivity and wind stress in a simple, coupled atmosphere-ocean carbon cycle, which builds on established thermocline theory. We consider two limit cases for thermocline circulation: the diffusive thermocline and the ventilated thermocline. In the limit of a purely diffusive thermocline (no wind-driven gyres), atmospheric pCO_2 increases in proportion to the depth of thermocline which scales as $\kappa^{1/3}$, where κ is the diapycnal mixing rate coefficient. In the wind-driven, ventilated thermocline limit, the ventilated thermocline theory suggests the thickness of the thermocline varies as $w_{ek}^{1/2}$. Moreover, surface residence times are shorter, and subducted waters are undersaturated. The degree of undersaturation is proportional to the Ekman pumping rate, w_{ek}, for moderate amplitudes of w_{ek}. Hence, atmospheric pCO_2 varies as $w_{ek}^{3/2}$ for moderate ranges of surface wind stress. Numerical experiments with an ocean circulation and abiotic carbon cycle model confirm these limit case scalings and illustrate their combined effect. The numerical experiments suggest that plausible variations in the wind forcing and diapycnal diffusivity could lead to changes in atmospheric pCO_2 of as much as 30 ppmv. The deep ocean carbon reservoir is insensitive to changes in the wind, due to compensation between the degree of saturation and the equilibrium carbon concentration. Consequently, the sensitivity of atmospheric pCO_2 to wind-stress forcing is dominated by the changes in the upper ocean, in direct contrast to the sensitivity to surface properties, such as temperature and alkalinity, which is controlled by the deep ocean reservoir.

1. Introduction

The partitioning of carbon between oceanic and atmospheric reservoirs and its dependence on the circulation and climate of the oceans has been studied extensively due to the likely role of the oceans in modulating atmospheric CO_2 on glacial-interglacial timescales (reviewed by Sigman and Boyle, 2000) and the current oceanic sink of fossil fuel CO_2 from the atmosphere (e.g. Gruber *et al.,* 1996). While it seems clear that the oceans play a significant role with regard to both of these issues, much remains to be understood.

1. Program in Atmospheres, Oceans and Climate, Massachusetts Institute of Technology, Cambridge, Massachusetts 02139, U.S.A. ***email: ito@gulf.mit.edu***

The inventory of carbons in the ocean is largely controlled by two important mechanisms: the solubility and biological pumps (Volk and Hoffert, 1985). The solubility pump reflects the temperature dependence of solubility of CO_2 and thermal stratification of the ocean. Cold deep waters are generally enriched in dissolved inorganic carbon (hereafter, *C*) in part due to their higher solubility. For a review of ocean carbonate system, see Stumm and Morgan (1996). The biological pump involves production and dissolution of organic molecules. Photosynthesis occurs in the euphotic layer, converting inorganic carbon and nutrients to organic matter. Some organic matter leaves the euphotic layer as sinking particles, and it is remineralized in the ocean interior. Both solubility and biological pumps tend to increase the deep water *C* concentration, creating a vertical gradient of *C*.

Box model studies in the 1980's supported the notion of a dominant role for the high latitude oceans in controlling atmospheric pCO_2 (Sarmiento and Toggweiler, 1984; Knox and McElroy, 1984; Siegenthaler and Wenk, 1984), largely through the biological pump. Recent studies with three-dimensional ocean circulation and biogeochemistry models (Bacastow, 1995; Broecker *et al.,* 1999; Archer *et al.,* 2000) suggest that atmospheric pCO_2 also shows a greater sensitivity to low latitude surface ocean properties than had previously been accepted. Archer *et al.* (2000) suggest that this might be due to the parameterizations of subgrid-scale mixing and diapycnal mixing in the ocean. Toggweiler *et al.* (2003) found that the sensitivity of atmospheric CO_2 to low latitude surface properties in box models depends on the representation of deep water formation, and showed that the box models can be sensitive to low latitudes by an adjustment in the area of high latitude surface ocean. Alternatively, Follows *et al.* (2002), using an idealized general circulation and abiotic carbon cycle model (Fig. 1), showed that the wind-driven circulation enhances the sensitivity of atmospheric pCO_2 to low latitude surface properties by creating a pool of relatively warm waters in the ventilated thermocline which inherit their properties from the mid-latitude surface. The model, which conserves the total amount of carbon in ocean and atmosphere, also illustrated a strong sensitivity of atmospheric pCO_2 to the presence or absence of wind forcing.

In Figure 1, we illustrate results from that numerical model, details of which may be found in Follows *et al.* (2002). Briefly, the experiments are performed with the MIT ocean model configured in a 60° longitude by 90° latitude basin at $3° \times 3°$ resolution, with 15 vertical levels. It is overlain by an abiotic carbon cycle model which is coupled to a simple atmospheric reservoir of CO_2. Carbonate chemistry is explicitly solved and the air-sea exchange of CO_2 is parameterized with a uniform gas transfer coefficient. In Follows *et al.* (2002), we compare experiments with thermohaline forcing only to those with both thermohaline and wind forcing. The meridional overturning circulation and thermal structure of the model in these two cases is shown in Figure 2. The model resolves the ventilated thermocline reasonably well. When wind forcing is present, the ocean gyres spin up and the warm lens of the subtropical thermocline develops. Though atmospheric pCO_2 increased with the introduction of the wind forcing, the mean ocean temperature (and therefore, solubility) did not change significantly. The increase in atmospheric CO_2 was

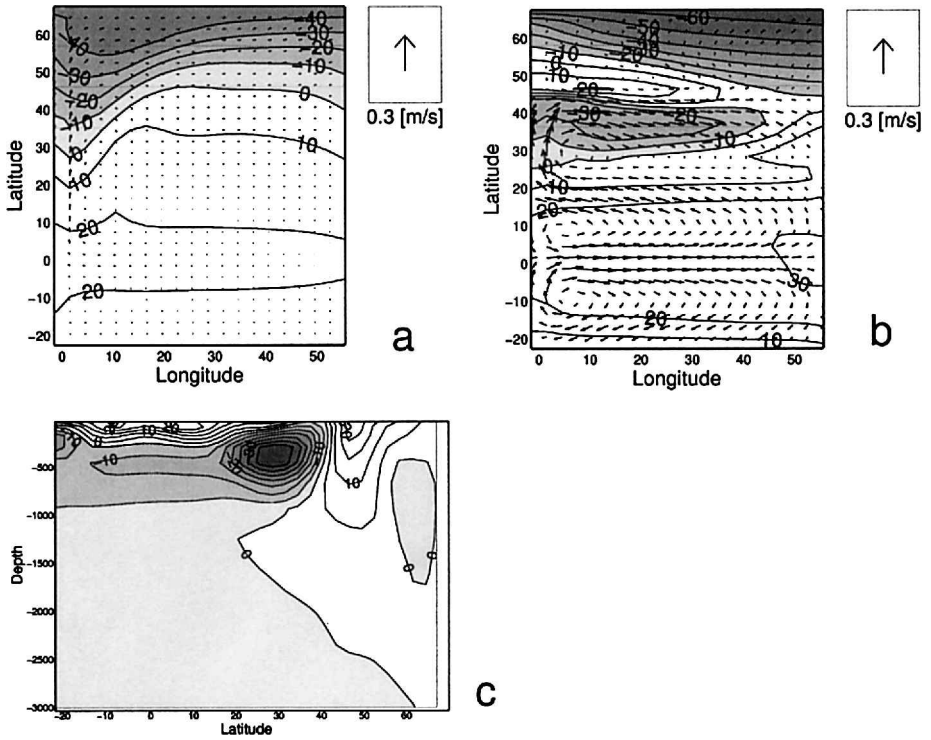

Figure 1. Abiotic sector model of ocean-atmosphere carbon cycle: (a) Surface currents and difference in partial pressure of CO_2 across the sea surface in the sector model *without* wind forcing. (b) Surface currents and difference in partial pressure of CO_2 across the sea surface in the sector model with strong wind forcing. (c) Difference in zonally averaged C concentration (mol m^{-3}) between the model with strong wind forcing and the model with no wind forcing.

attributable to the waters of the subtropical thermocline becoming significantly undersaturated. The surface currents are slow in the model without wind-forcing (Fig. 1a), the residence time of water parcels at the surface is long, and the surface ocean is close to equilibrium with the atmosphere. In the wind-driven model the surface currents are swift (Fig. 1b), the air-sea equilibration time scale and the residence time of surface waters are comparable. Waters of the ventilated thermocline are significantly undersaturated due to the strong cooling in the western boundary current. Since the thermocline is depleted in C, by mass conservation, carbon must be transferred to the atmosphere. Figure 1c illustrates the difference in C in the upper ocean between the two cases.

These numerical experiments suggested a potentially significant role for the ventilated thermocline in modulating atmospheric CO_2 on decadal and longer timescales, but motivates the broad questions: What are the physical controls on the solubility pump of carbon in the oceans? Can we provide a general theory of its dependence on wind-stress

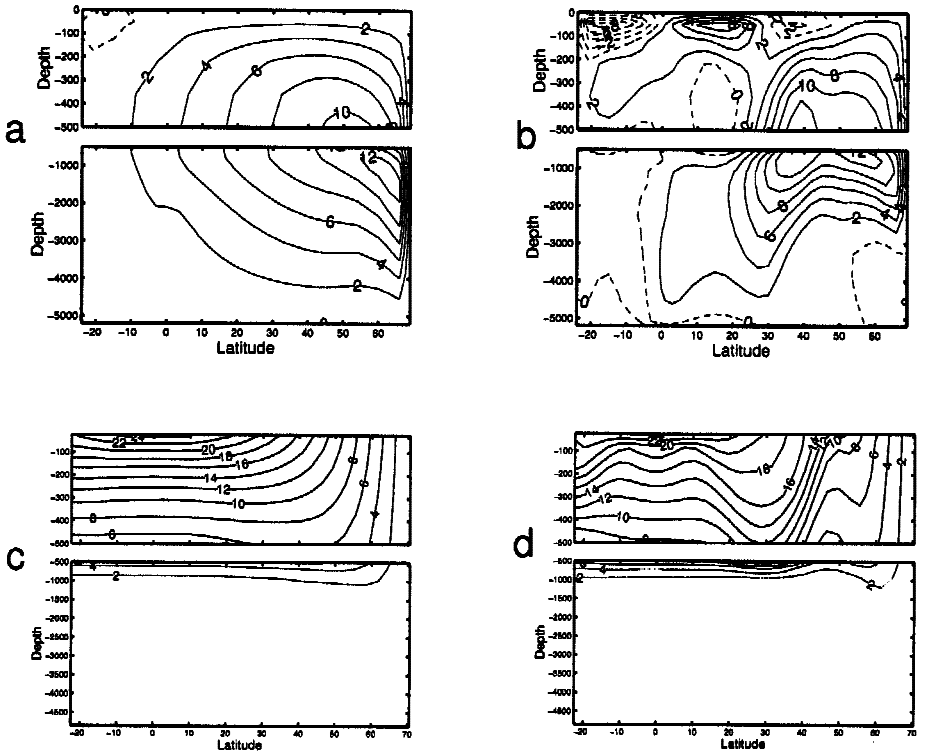

Figure 2. Meridional overturning circulation (Sv) and potential temperature (°C) for the sector model (a, c) without wind forcing and (b, d) with strong wind forcing (maximum wind-stress 0.2 N m^{-2}).

forcing and diapycnal mixing rates? How might the solubility pump respond to climatic change, through changes to these physical properties?

In this study we seek to understand how the physical structures and processes of the ocean control the solubility pump of CO_2. For simplicity and clarity we focus on an abiotic ocean. We develop scalings which relate the storage of carbon in the ocean and, thus, atmospheric pCO_2 to diapycnal mixing and Ekman pumping rates. We demonstrate that these scalings accurately predict the behavior of an idealized, three-dimensional, ocean-atmosphere carbon cycle model (Follows *et al.,* 2002). Over a reasonable range of diapycnal diffusivity and wind-stress, atmospheric pCO_2 varies by as much as 30 ppmv. This suggests a possibly significant role for the wind-driven gyres in modulating atmospheric CO_2 on decadal timescales, and even with regard to glacial-interglacial change. It also provides the basis for a deeper understanding of the differences between more complex numerical simulations of the oceans.

In Section 2 we review the mass balance of carbon in a simplified, abiotic ocean-atmosphere system. In Section 3 we briefly review some relevant aspects of the theory of

thermocline thickness. We outline the scaling arguments which relate atmospheric pCO_2, diapycnal mixing and Ekman pumping in Section 4, and demonstrate that these scalings hold true in the setting of the numerical model. We also demonstrate that the upper ocean, and not the deep oceans, control the sensitivity of atmospheric CO_2 to changes in surface wind-stress. Finally, we discuss the relevance of this theory for more realistic models and for our understanding of the links between climate change and biogeochemistry.

2. Partitioning of carbon between ocean and atmosphere: Abiotic ocean limit

The hydrographic structure of the oceans, in combination with the alkalinity and buffering carbonate chemistry, determines its carbon loading capacity at thermodynamic equilibrium. The thickness of thermocline controls the relative volume of the warm, upper oceans and the cold, deep oceans. For example, a deeper thermocline implies higher ocean heat content and lower carbon loading capacity. The ability of the ocean to actually achieve this potential carbon loading is determined by the equilibration state of the waters which ventilate the thermocline and the deep ocean. The degree of saturation depends on the competition between the residence time of surface water parcels, the surface heat forcing and the air-sea gas equilibration time scale. The characteristic time scale for air-sea CO_2 equilibration of the mixed layer is on the order of a year. If the surface residence time is much longer than a year, the parcel is close to thermodynamic equilibrium with atmospheric pCO_2.

First, we briefly define the ocean-atmosphere carbon balance in the framework of a 2-box model (Fig. 3). The solubility pump may be understood in terms of the volumes, temperatures and carbon concentrations of the deep ocean and the thermocline box. For a closed system (neglecting river input and sediment burial), mass balance dictates that atmospheric pCO_2 will vary in response to changes in the volume and properties of these reservoirs. A statement of mass balance for this simplified ocean with a warm, thermocline layer of C concentration, C_{th}, overlying a cool, deep ocean layer, with C concentration, C_d, is

$$Mp\mathrm{CO}_2^{at} + V_d C_d + V_{th} C_{th} = C_{total} \tag{1}$$

where M is the total moles of gases in the atmosphere, and $p\mathrm{CO}_2^{at}$ is the mixing ratio of CO_2 in the atmosphere. V_d and V_{th} are the volumes of the deep ocean and thermocline, respectively. Note that the upper ocean layer is assumed to be the thermocline and not the surface mixed layer. C_{total} is the total amount of carbon in this closed, atmosphere-ocean system. Hence, from (1),

$$p\mathrm{CO}_2^{at} \propto -(V_d C_d + V_{th} C_{th}). \tag{2}$$

Assuming that the thermocline box and the deep ocean box have the same area, the relative volume of these boxes is equal to the relative thickness, $V_{th}/V_d = h/(H - h)$. The deep waters represent the leading order control on $p\mathrm{CO}_2^{at}$. At the next order, $O(h/H)$, the

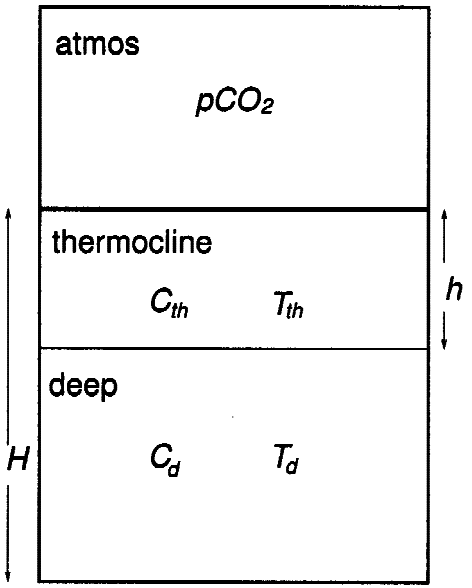

Figure 3. Schematic two-box ocean and atmosphere carbon cycle model. The depth of the ocean is set to a constant, $H(m)$. The top box is the atmospheric reservoir of CO_2 with its total moles M (mol). The middle box represents thermocline (upper ocean) which is warm with temperature T_{th} and C concentration C_{th}. The depth of thermocline is $h(m)$. The deep box represents abyssal ocean with is cold with temperature T_d and C concentration C_d.

column C inventory depends linearly on the thickness of thermocline, h. For example, all else being equal, an increase in the thickness of thermocline results in the linear reduction of the storage of carbon in the ocean.

3. Diffusive and ventilated thermocline

In order to understand the role of the thermocline as a carbon reservoir, we must first consider what controls its thickness and hydrographic structure. The dynamics of the ocean's thermocline have been extensively studied with two-limit cases for thermocline circulation: the diffusive thermocline and the ventilated thermocline. In a diffusively controlled thermocline, large-scale upwelling of cold waters is balanced by downward diapycnal mixing of heat. In a ventilated thermocline, Ekman pumping and surface buoyancy gradients dictate upper ocean structure. It is beyond the scope of the present study to discuss thermocline theory in depth. We refer the reader to a review by (Pedlosky, 1986) and the paper of (Vallis, 2000) on this topic. The two views of the thermocline, depicted schematically in Figures 4 and 5, are not necessarily exclusive. Recent studies have viewed the thermocline as reflecting a combination of these processes (Samelson and Vallis, 1997). We find some evidence of the two thermocline regimes occurring simulta-

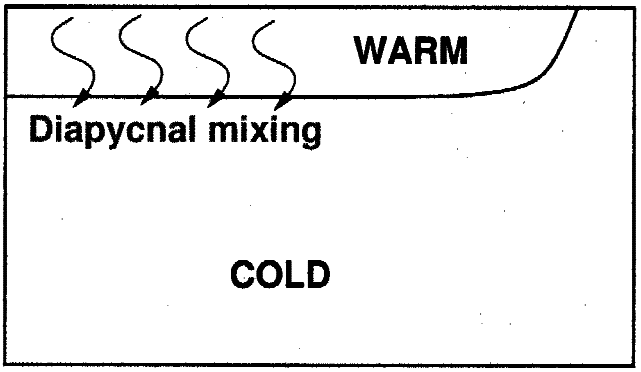

Figure 4. A schematic diagram for diffusive thermocline in an ocean basin.

neously in our numerical simulations when diapycnal diffusivity is sufficiently small. Figure 2(d) shows some characteristics of an upper, ventilated thermocline overlying an internal, diffusive thermocline.

Here we develop scalings for the carbon system in both the diffusive and ventilated thermocline limits, and examine these scalings in the context of a numerical model which has both explicit diapycnal mixing and wind-stress forcing, and thus may be influenced by both mechanisms.

Scalings relating thermocline depth and diapycnal mixing in a wind-free ocean have been developed and demonstrated to be consistent with basin-scale ocean circulation models (Bryan 1987; Zhang *et al.,* 1999; Marotzke and Scott, 1999; Scott, 2000; Park and Bryan, 2000). These studies show that, in the absence of wind forcing, the meridional overturning rate and the depth of thermocline h can be related to diapycnal diffusivity through a simple scaling relationship. We assume that the surface buoyancy is prescribed

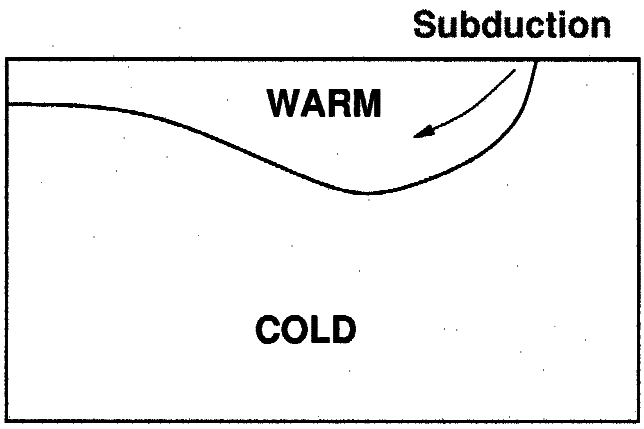

Figure 5. A schematic diagram for ventilated subtropical thermocline in an ocean basin.

as Δb (in numerical simulations, we use restoring boundary condition with a rapid damping rate), and also assume that the circulation is in geostrophic and hydrostatic balance. Diapycnal diffusivity is denoted by κ (m^2/s). In this diffusive limit

$$h \propto \kappa^{1/3} \Delta b^{-1/3}. \tag{3}$$

Figure 4 illustrates schematically the diffusive thermocline. Downward diffusion of heat balances the broad upwelling of cold, deep waters across the basin.

In contrast, other studies have examined the thermocline in an inviscid, wind-driven limit (Luyten *et al.,* 1983). In this limit, the thickness of the thermocline scales with the Ekman pumping rate

$$h \propto w_{ek}^{1/2}. \tag{4}$$

Figure 5 illustrates schematically the bowl of the warm subtropical thermocline. Wind-forcing induces Ekman transport and the gyre circulations of the upper ocean, creating a ventilated thermocline, the properties of which are set by subduction from the surface waters (e.g. Iselin, 1939; Stommel, 1979; Marshall *et al.,* 1993). In the ventilated thermocline limit (where diapycnal mixing is relatively small) the subtropical thermocline is formed of warm, carbon-depleted surface waters advected into the interior from the surface.

These views of the thermocline, and the scalings and numerical experiments presented here, are particularly relevant to the ocean basins. However, the zonally unblocked Antarctic Circumpolar Current represents an important ocean region with different dynamics. Gnanadesikan (1999) develops a global view of thermocline thickness, ocean heat content and overturning circulation. It is interesting and possible to consider the thermocline in the circumpolar channel, but it is beyond the scope of this study.

4. Carbon scalings and numerical experiments

In this section, we outline scalings for the relationship between atmospheric pCO_2 and physical parameters of an idealized, abiotic ocean and illustrate these scalings using numerical experiments with the single hemispheric sector ocean model briefly described in the Introduction and in more detail by Follows *et al.* (2002). In all simulations, surface buoyancy is restored to a prescribed meridional profile with a rapid, characteristic time scale of one month. The total carbon inventory of ocean-atmosphere system, C_{total}, is held constant in all simulations, which allows us to apply the simple carbon mass balance described in (1). Diapycnal diffusivity and the amplitude of surface wind-stress are varied for sensitivity experiments.

a. Diffusive thermocline

Here we examine the relationship between diapycnal mixing rates and atmospheric pCO_2 in the diffusive thermocline limit. Figure 4 schematically illustrates a diffusive

thermocline sustained by broad scale upwelling and diapycnal mixing. Likewise, in this case, C_{th} is determined by the balance between the upwelling of deep water and the downward diffusion of surface water properties. A prognostic equation for dissolved inorganic carbon for this abiotic system can be written

$$\frac{\partial C}{\partial t} + \nabla \cdot (\mathbf{u}C) = \nabla \cdot (\mathbf{K}\nabla C) - \frac{\Delta C}{\tau_c}. \tag{5}$$

where we define ΔC to be the departure of dissolved inorganic carbon from the value it would have at equilibrium with the overlying atmosphere, were it brought to the surface at its current temperature.

$$\Delta C = C - C_{eq}. \tag{6}$$

The first term on the r.h.s. of (5) is the eddy turbulence flux term, and the second term describes the air-sea CO_2 flux as a damping toward the equilibrium value, C_{eq}. The damping timescale, τ_c, depends on the gas transfer coefficient, the Revelle factor and ionization fractionation. For a mixed layer of thickness, $h_{ml} \sim 100$ m, τ_c is typically about one year (Broecker and Peng, 1974) but will vary with environmental factors.

At steady state, the horizontally averaged surface C must be equal to the horizontally averaged C_{eq} so that the net, global air-sea CO_2 flux is zero. In an ideal case where the diapycnal mixing can be described by a uniform diffusion coefficient and the isopycnals are mostly horizontal, the situation is best described in terms of the horizontally-averaged carbon balance equation. For the mixed layer,

$$\bar{C}(z = 0) = \bar{C}_{eq} \tag{7}$$

where $\bar{C}$ represents the horizontally-averaged C concentration. We consider the horizontal average of (5), which is a vertical advection-diffusion equation. We assume that the vertical velocity, $\bar{w}$, is a constant and the solution can be found with appropriate boundary conditions.

$$\bar{C}(z) = \bar{C}_{deep} - [\bar{C}_{deep} - \bar{C}(z = 0)]e^{z/h}. \tag{8}$$

The thickness of diffusive thermocline, h, is determined by $h = \kappa/\bar{w}$, which is the ratio between the diapycnal diffusivity and the vertical velocity. The top boundary condition comes from (7). The bottom boundary condition is set to $\bar{C}(H) = C_{deep}$, and we assume that $H \gg h$. The deep water carbon concentration, C_{deep}, is determined by the surface water properties at the location of deep water formation, and is assumed to be independent of κ.

Integrating (8) vertically we obtain the column C inventory,

$$\int_{-H}^{0} \bar{C}(z)dz \cong H\left[\bar{C}_{deep} - \frac{h}{H}(\bar{C}_{deep} - \bar{C}(z = 0))\right]. \tag{9}$$

This relationship reflects the simplified, two-box view suggested by (2). The ocean carbon inventory is mainly determined by the deep waters because of its large volume, as one might expect. The impact of the thermocline reservoir enters at the order of $O(h/H)$. Increasing the depth of thermocline results in a net warming of the ocean and reduction of the potential for ocean carbon storage.

Combining (3) and (9), the storage of carbon in the ocean can be seen to be proportional to the cubed root of the diapycnal diffusion coefficient:

$$\int_{-H}^{0} \bar{C}(z)dz \propto -\kappa^{1/3}. \tag{10}$$

Adding the constraint of carbon conservation, (1), we see the relationship of atmospheric $p\mathrm{CO}_2$ and the diapycnal mixing coefficient, κ.

$$\boxed{p\mathrm{CO}_2^{at} \propto \kappa^{1/3} \quad \text{for } w_{ek} = 0.} \tag{11}$$

In this diffusive thermocline limit, steady-state atmospheric $p\mathrm{CO}_2$ is predicted to vary as the cubed root of diapycnal diffusivity. Since the degree of saturation is independent of κ in this limit, $p\mathrm{CO}_2^{at}$ is simply controlled by the modulation of the thickness of the warm, carbon-depleted thermocline. The two-dimensional numerical experiments of (Archer *et al.,* 2000) illustrate, in part, this sensitivity to diapycnal mixing rates.

i. Numerical experiments of the diffusive thermocline. We may ask whether the relationship between diapycnal mixing and atmospheric $p\mathrm{CO}_2$ predicted in (11) holds in a more complex setting. To test this we use an ocean general circulation and an abiotic carbon model, configured in a simple, single-hemisphere basin, and connected to a well-mixed atmospheric reservoir of CO_2. The model, as configured here, is described in more detail in (Follows *et al.,* 2002). The total carbon budget of the ocean-atmosphere system is conserved and atmospheric $p\mathrm{CO}_2$ adjusts with ocean circulation according to its influence on the oceanic carbon reservoir. C is carried as a tracer in the model and air-sea gas transfer coefficient and surface alkalinity are prescribed as spatially uniform values. The model is initialized with uniform distribution of buoyancy and C, and spun up to steady state.

Figure 1a shows the distribution of $\Delta p\mathrm{CO}_2$, the $p\mathrm{CO}_2$ difference between the ocean and atmosphere, in the control spin up of the model where $\kappa = 5 \cdot 10^{-5}\ \mathrm{m^2\,s^{-1}}$ and the wind stress is set to zero everywhere. There is a broad tropical and subtropical region of outgassing associated with the upwelling and warming of cool, carbon rich deep waters. CO_2 is absorbed from the atmosphere at subpolar latitudes and along the path of the western boundary current where there is strong cooling of the surface waters. In the absence of wind forcing, the surface currents and subduction rates are relatively slow, and $\Delta p\mathrm{CO}_2$ has moderate values. For the control experiment steady state atmospheric $p\mathrm{CO}_2$ is 269 ppmv, arbitrarily determined by the imposed total ocean-atmosphere budget of carbon. Here we seek to understand the sensitivity of atmospheric $p\mathrm{CO}_2$ to small changes in the

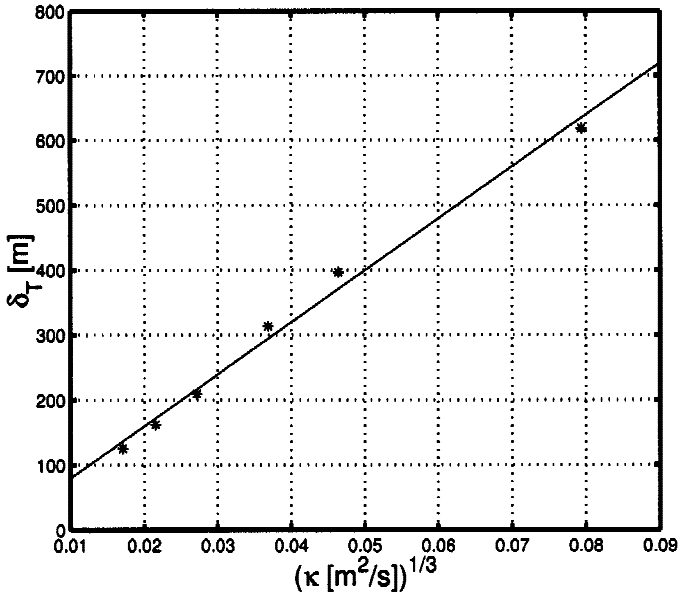

Figure 6. Steady state sensitivity of thermocline depth, δ_T, to diapycnal mixing rate in the sector model in the diffusive thermocline limit (no wind forcing). Simulated thermocline depth, δ_T, is diagnosed from the steady state temperature field following Park and Bryan (2000). The steady state thermocline depth scales with the cubed root of the diapycnal diffusivity, consistent with the scaling theory.

physical parameters. The sector model is integrated to new steady states for a range of κ spanning over two orders of magnitude but with the same buoyancy boundary conditions as the control run.

Simulated temperature fields confirm the cubed root dependence of thermocline depth to diapycnal diffusivity. Figure 6 shows the relationship between κ and the simulated thermocline depth, δ_T, which is diagnosed from the modeled fields following the definition of Park and Bryan (2000).

$$\delta_T(x, y) = \frac{\int_{bottom}^{top} (T - T_{bottom}) z dz}{\int_{bottom}^{top} (T - T_{bottom}) dz} \tag{12}$$

In Figure 6, the values of δ_T are obtained from zonal averages at 30N.

Figure 7 shows the relationship between the steady atmospheric pCO_2 and κ. The result is in excellent agreement with the scaling analysis of (11) with atmospheric pCO_2 varying as $\kappa^{1/3}$.

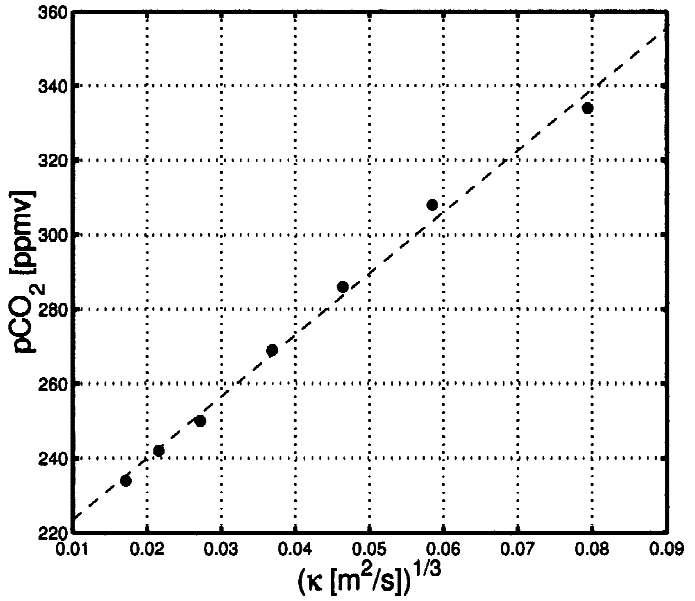

Figure 7. Steady state sensitivity of atmospheric pCO_2 to diapycnal mixing rate in the sector model in the diffusive thermocline limit (no wind forcing). Each dot in the plot represents simulations with different diapycnal diffusivity, and the line is the least square fit to these points. Diapycnal diffusivities, κ, are varied over two orders of magnitude. The steady state atmospheric pCO_2 scales with the cubed root of the diapycnal diffusivity, and the modeled sensitivity is in an excellent agreement with the simple theory.

The sector model supports the qualitative and quantitative predictions of the scaling. Since the simulated upper ocean currents are weak without the surface wind-stress forcing (Fig. 2), the surface buoyancy distribution is close to the prescribed meridional profile, though there is a small departure in our simulations, and its magnitude increases with κ. However, the deviations of the surface buoyancy from the prescribed value are very small for a reasonable range of κ, and the sensitivity of atmospheric CO_2 is largely determined by the volume (or thickness) of the thermocline which scales as $\kappa^{1/3}$.

b. The ventilated thermocline

In the previous section we developed a simple scaling that successfully predicts the relationship between diapycnal mixing and atmospheric pCO_2, in an abiotic ocean in the absence of wind forcing. What is the influence of wind forcing on the carbon inventory of the ocean and atmospheric CO_2? The magnitude of the carbon reservoir in the ventilated thermocline is a function of the volume of thermocline waters and their carbon content—see (2).

Theory and numerical models have shown that in a closed basin, thermocline thickness

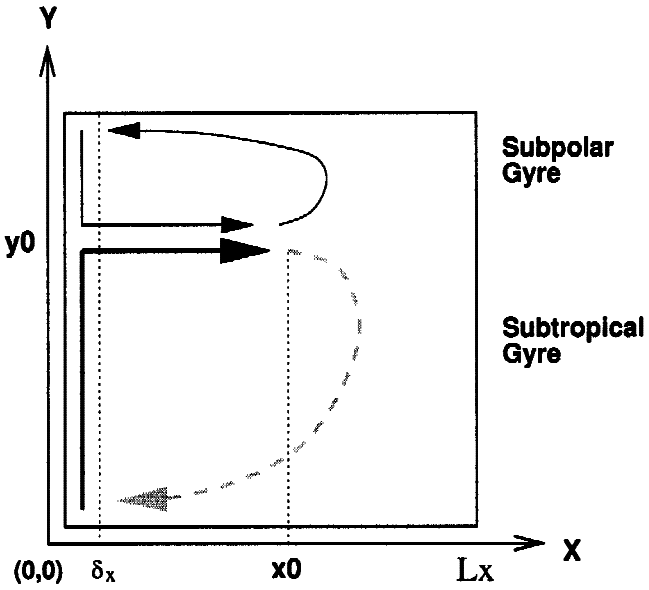

Figure 8. A schematic diagram for ventilated subtropical thermocline in an ocean basin. In subtropical gyre, we consider an idealized path of the western boundary current. δ_x is the width of the western boundary current, and L_x is the width of the basin. Northward flow has the velocity of v (m s^{-1}) from (0, 0) to (0, y_0), then it separates from the coast and moves toward (x_0, y_0) with the velocity of u (m s^{-1}).

(or volume, assuming constant surface area) varies as the square root of the amplitude of the wind-stress forcing, τ (Luyten *et al.,* 1983):

$$V_t \propto h \propto w_{ek}^{1/2}. \tag{13}$$

In an inviscid, wind-driven ocean, the thermocline waters are formed in the subduction regions from where they are advected into the interior. As illustrated in Figure 1, surface currents are considerably swifter in the wind-driven ocean. The residence time of waters in the mixed layer is, therefore, shorter and water parcels may be subducted while still far from equilibrium with the atmosphere. For the wind-driven ocean we must also evaluate the impact of this short residence time on the saturation state and carbon concentration in the subducted thermocline waters.

i. What sets the C of the abiotic, ventilated thermocline? Figure 8 depicts idealized pathways of water parcels in the subtropical and subpolar gyres of the northern ocean basins. In the subtropics, a water parcel travels northward in the western boundary current, separating from the western boundary at $y = y_0$ where the curl of the wind stress vanishes. The water travels eastward to the point (x_0, y_0) where it is subducted beneath the surface layer. After subduction, the water parcel is no longer in contact with the atmosphere, so

carbon is conserved, and it travels downward and southward along the trajectory indicated by a dashed line. Such trajectories can be calculated from the surface wind stress explicitly (Luyten *et al.,* 1983). Hence, for the abiotic case, the carbon stored in the subtropical thermocline is determined by the C concentration at the point of subduction.

We first consider the carbon balance in the mixed layer by integrating (5) vertically from the surface to the base of the mixed layer. For simplicity, we assume a prescribed, constant mixed layer depth of h_{ml}. Considering the flux balance at the base of the mixed layer, we find an equation for the surface carbon balance.

$$\frac{DC}{Dt} + \wedge \frac{w}{h_{ml}}(C - C_{ent}) = -\frac{\Delta C}{\tau_c} \tag{14}$$

where D/Dt is the total derivative following a parcel including the effect of horizontal advection. Vertical advection is represented by the entrainment term on the l.h.s. of (14), which is active only when the water is upwelling. $\wedge$ is 1 if w is positive (upwelling); 0 elsewhere (downwelling) as it is in the subtropical gyres. C_{ent} represents the concentration just below the base of mixed layer. We rewrite (14) in terms of ΔC using (6), and find an expression for the change in the carbon disequilibrium, ΔC, following a water parcel as it moves around the surface ocean:

$$\frac{D\Delta C}{Dt} + \wedge \frac{w}{h_{ml}}(C - C_{ent}) = -\frac{\Delta C}{\tau_c} - \frac{DC_{eq}}{Dt}. \tag{15}$$

The air-sea gas transfer term is expressed as a damping toward equilibrium or an exponential decay of ΔC. We have additional forcing on the r.h.s., which is expressed as the change of C_{eq} following the water parcel, DC_{eq}/Dt, reflecting changes in temperature, salinity or alkalinity of the water parcel during its transit. This Lagrangian framework is derived in more detail, including a treatment of biological influences, by Follows and Williams (2003). Here, we assume that alkalinity and salinity of waters are uniform in space and time, and C_{eq} varies only with atmospheric $p\mathrm{CO}_2$ and sea-surface temperature. We also assume a steady, well-mixed atmosphere. The prescribed SST distribution is a function of latitude only. Thus we may take an idealized view in which C_{eq} varies only with latitude.

$$\frac{DC_{eq}}{Dt} = \frac{\partial C_{eq}}{\partial t} + \mathbf{u}_H \cdot \nabla_H C_{eq} \sim v\frac{\partial C_{eq}}{\partial y}. \tag{16}$$

Combining (15) and (16), we find a simplified equation for the evolution of ΔC.

$$\frac{D\Delta C}{Dt} + \frac{\Delta C}{\tau_c} = -v\frac{\partial C_{eq}}{\partial y}. \tag{17}$$

Here, we assume that the entrainment term is zero since Ekman pumping is downward in the subtropical gyre. Also, the meridional velocity, v, and the gradient, $\partial C_{eq}/\partial y$, are

assumed to be constant. This expression (17) can be integrated analytically following the trajectory of the water parcel in the surface mixed layer, from an initial location in the tropics to the point of subduction. The pathway in the surface consists of two parts; (1) the western boundary current, and (2) the interior gyre circulation. For simplicity, we assume that the western boundary current is purely meridional with velocity v and the interior trajectory is purely zonal to the point of subduction, (x_0, y_0), with velocity u, as depicted in Figure 8.

The general solution for (17) is

$$\Delta C(x(t), y(t)) = \Delta C(t = 0)e^{-t/\tau_c} + (v\tau_c)\frac{\partial C_{eq}}{\partial y}(e^{-t/\tau_c} - 1) \tag{18}$$

where t is the time since the parcel started its transit through the western boundary current system at $(x, y) = (0, 0)$ with initial carbon anomaly $\Delta C(t = 0)$. The first term represents the influence of the initial condition, which exponentially decays with time. The second term represents the solubility change associated with the meridional advection of a water parcel. We define the time interval in which the parcel transits from (0, 0) to $(0, y_0)$ as $t_0 \equiv y_0/v$, and the transit time from $(0, y_0)$ to (x_0, y_0) as $t_1 \equiv x_0/u$. For this idealized pathway we find an expression for the carbon anomaly (local disequilibrium) at the location of subduction, $(x, y) = (x_0, y_0)$. We apply (18) separately to two intervals, from (0, 0) to $(0, y_0)$, and from $(0, y_0)$ to (x_0, y_0). The combined result is

$$\Delta C(x_0, y_0) = \left[\Delta C(t = 0)e^{-t_0/\tau_c} + (v\tau_c)\frac{\partial C_{eq}}{\partial y}(e^{-t_0/\tau_c} - 1)\right]e^{-t_1/\tau_c}. \tag{19}$$

$\Delta C(x_0, y_0)$ is the degree of saturation at the location of the subduction. Subduction may occur in various longitudes, and x_0 can have a range over the longitudinal width of the basin, suggesting that the magnitude of $\Delta C(x_0, y_0)$ is the greatest near the western boundary, and exponentially decreases eastward. When water masses subduct into the thermocline, C is conserved following the parcel in this abiotic limit and in absence of diapycnal mixing. Thus, the carbon concentration of the ventilated thermocline can be expressed as $C(x_0, y_0) = C_{eq}(x_0, y_0) + \Delta C(x_0, y_0)$, where $C_{eq}(x_0, y_0)$ is a function of local temperature, salinity and alkalinity. We examine two limits of the solution (19): the slow transport limit where the transit time of the water parcel through the western boundary current system is comparable to the air-sea equilibration timescale, and the fast transport limit where the transit is very fast relative to air-sea equilibration.

ii. Weak wind forcing and slow transport. If the wind-stress curl is sufficiently weak the transit time along the western boundary current system is much longer than the timescale for air-sea equilibration of pCO_2; $t_0 \gg \tau_c$. In this case, we assume $e^{-t_0/\tau_c} \ll 1$ and $\Delta C(x_0, y_0)$ becomes independent of the initial condition. (19) simplifies to

$$\Delta C(x_0, y_0) \sim -\left[(v\tau_c)\frac{\partial C_{eq}}{\partial y}\right]e^{-t_1/\tau_c} \quad t_0 \gg \tau_c. \tag{20}$$

In this limit, the water parcel resides in the surface long enough to "forget" the initial disequilibrium at the beginning of its boundary current transit. The form of (20) suggests that $\Delta C(x_0, y_0)$ is proportional to the product of v, τ_c, and $\partial C_{eq}/\partial y$. In the boundary current, v is positive (northward), τ_c, is set by the gas exchange coefficient and carbonate chemistry, and $\partial C_{eq}/\partial y$ depends on the relationship of solubility to temperature and the SST distribution. Solubility decreases with temperature, $\partial C_{eq}/\partial T < 0$, and the meridional temperature gradient, $\partial T/\partial y$, is negative in the northern hemisphere, $\partial T/\partial y < 0$. Using the chain rule, $\partial C_{eq}/\partial y = (\partial C_{eq}/\partial T)\,(\partial T/\partial y) > 0$, thus we find a positive gradient of C_{eq} in the northern hemisphere.

The disequilibrium at the point of subduction is controlled by the competition between integrated forcing (i.e. cooling) along the trajectory of the water parcel and the damping effect of air-sea gas exchange. Cooling along the boundary current is associated with the downstream uptake of CO_2. Air-sea CO_2 flux lags the air-sea heat flux due to the difference in timescales between gas exchange and heat exchange. An intensification of the boundary current enhances undersaturation of the parcel due to the rapid cooling and its associated solubility increases. An increase in gas exchange timescale also enhances the disequilibrium, ΔC, because of the greater lag between the cooling and the CO_2 uptake, see (18).

Assuming that the western boundary current is passively closing the interior gyre circulation, v, is simply proportional to the subtropical Ekman pumping rate, w_{ek}. Considering Sverdrup's equation (see Chapter 1 and 2 of Pedlosky (1996) for reference), the northward velocity in the boundary current is

$$v = \frac{f}{\beta}\frac{L_x}{\delta_x}\frac{w_{ek}}{H} \tag{21}$$

where δ_x is the width of the western boundary current, L_x is the longitudinal width of the basin. The speed of the boundary current, v, is determined by the Ekman pumping rate. Thus, from (20), the C of the ventilated thermocline varies linearly with Ekman pumping in this slow transport regime:

$$C_{th} = C(x_0, y_0) \propto -w_{ek} \quad t_0 \gg \tau_c. \tag{22}$$

Combining the dependencies of thermocline thickness, (13), and subducted carbon concentration, (22), on Ekman pumping, and enforcing conservation of carbon in the ocean-atmosphere system, (2), we find for this slow transport (weak wind stress) limit, the dependence of atmospheric pCO_2 on the subtropical Ekman pumping:

$$\boxed{pCO_2^{at} \propto w_{ek}^{3/2} \quad \text{for } t_0 \gg \tau_c} \tag{23}$$

iii. Strong wind forcing and rapid transport. In the limit of strong wind forcing, the transit of the water parcel from tropics to subduction is fast relative to the air-sea CO_2 exchange, $t_0 \ll \tau_c$, and

$$\Delta C(x_0, y_0) \sim \left[\Delta C(0) - y_0 \frac{\partial C_{eq}}{\partial y} \right] e^{-t_1/\tau_c} \quad t_0 \ll \tau_c. \tag{24}$$

Because of the rapid advection, C is largely unchanged by the air-sea exchange of carbon which is too slow. The parcel also undergoes significant cooling, so is considerably undersaturated at the point of subduction and largely reflects the initial condition at the beginning of the western boundary current transit:

$$C_{th} = C(x_0, y_0) \sim C(0, 0) \quad t_0 \ll \tau_c. \tag{25}$$

In this limit, assuming that $C(0, 0)$ is independent of the wind forcing, the budget of carbon in the ventilated thermocline, $V_{th}C_{th}$, is modulated only by variations in thermocline thickness, which varies as $w_{ek}^{1/2}$ following (13) (Luyten *et al.,* 1983). An increase in wind forcing increases the depth of the thermocline and increases the volume of warm thermocline waters. Hence the ocean carbon budget is decreased and atmospheric pCO_2 increases. Combining (2), (13) and (25), the steady state atmospheric pCO_2 is proportional to the square-root of Ekman pumping in the strong wind limit.

$$\boxed{pCO_2^{at} \propto w_{ek}^{1/2} \quad \text{for } t_0 \ll \tau_c} \tag{26}$$

An increase in the wind stress deepens the ventilated thermocline, and the increase in the volume of warm, thermocline water decreases ocean carbon inventory, which results in an increase in atmospheric pCO_2.

The slow and rapid transport regimes are separated at a critical timescale where a surface water parcel reaches local equilibrium with overlying atmospheric pCO_2 under current physical conditions. This is on the order of one year. For the ocean's subtropical gyres, with dimension ($y_0 \sim 3000$ km), the critical western boundary current speed marking the regime shift is therefore about 0.1 m s^{-1}, which is of similar order to the mean speed of the present Gulf stream or Kuroshio.

In brief summary: Atmospheric pCO_2 depends on the wind-driven ocean circulation through its control on the volume of the ventilated thermocline and through its control on the saturation state of subducted waters. For relatively weak wind forcing, pCO_2 reflects both of these influences and scales as $w_{ek}^{3/2}$. For strong Ekman pumping rates, the western boundary current becomes very swift and the saturation state of the waters of the ventilated thermocline no longer depends on the residence time of surface water parcels. In this fast transport limit, pCO_2 scales with $w_{ek}^{1/2}$.

iv. Wind-driven gyre: Numerical experiments. Do the scalings for the ventilated thermocline hold up in the numerical sector model? Figure 1b shows ΔpCO_2, the air-sea difference, in a wind-driven integration of the model. In that case the maximum wind-stress is set to 0.2 N m^{-2} with diapycnal diffusivity of $5 \cdot 10^{-5}$ m^2 s^{-1}. As noted in (Follows *et al.,* 2002), upwelling and outgassing are now confined to the tropics, and the subtropical air-sea flux changes sign relative to the case with thermohaline forcing only.

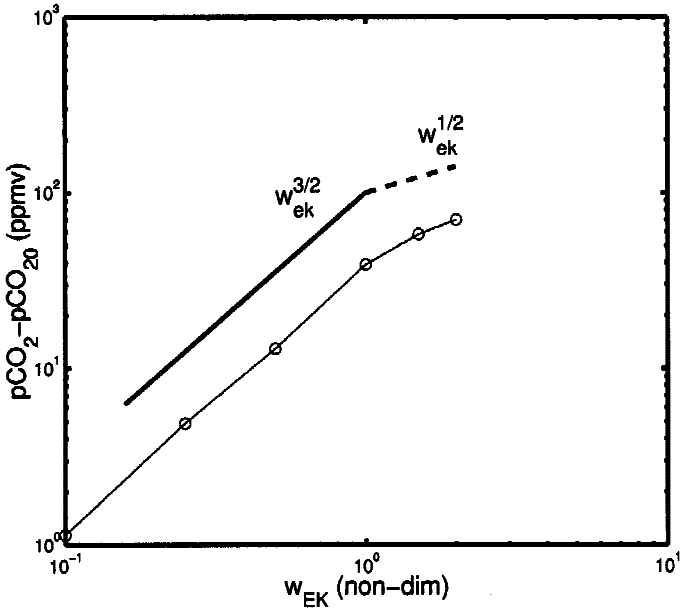

Figure 9. The relationship between the wind stress amplitude and the atmospheric pCO_2 calculated by the idealized GCM. Scalings (23), (26) are in excellent agreement with the modeled sensitivities. Horizontal axis represents nondimensionalized magnitudes of Ekman pumping. The case $w_{ek} = 1$ (non − dim) corresponds to the simulation with the westerly wind-stress maximum of 0.2 N m^{-2}. Spatial pattern of wind stress is prescribed, and its amplitudes are varied. The vertical axis is the difference in pCO_2 between the run with wind amplitude, τ, and the control run (no wind, $\tau = 0$).

The western boundary current, which is rapidly losing heat, becomes undersaturated with CO_2. The undersaturated water drives the downstream oceanic uptake of carbon from the atmosphere as predicted by the simple theory. This is consistent with the observed uptake of carbon by the subtropical gyres (Takahashi *et al.,* 1997) and more realistic models (Follows *et al.,* 1996). The region of net ocean outgassing near the intergyre boundary at mid-latitudes is due to the cyclonic circulation of the subpolar gyre feeding carbon rich subpolar waters to warmer mid-latitudes.

We use the numerical model to find the steady state pCO_2^{at} for a range in amplitude of the wind stress forcing. τ, the maximum wind-stress, was varied from 0.1 N m^{-2} to 0.4 N m^{-2} keeping the spatial pattern the same. Though the theory is developed for an inviscid ocean, a finite diapycnal mixing rate of 10^{-5} m^2 s^{-1} was imposed. Total ocean and atmosphere carbon was conserved. The results of the individual experiments are depicted in Figure 9 along side the theoretical predictions for the slow, (23), and fast, (26), transport regimes, assuming the critical maximum wind-stress to be at 0.2 N m^{-2}. The numerical model results are clearly consistent with the predicted scalings: When the wind stress forcing is weaker than 0.2 N m^{-2}, atmospheric pCO_2 scales as $\tau^{3/2}$. At maximum

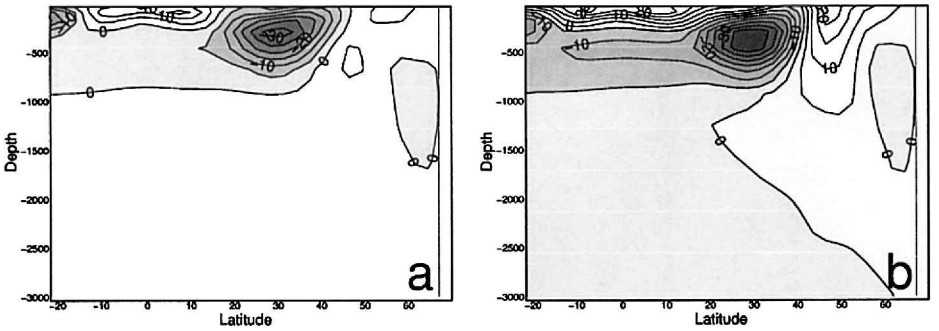

Figure 10. Change in zonally averaged C concentration in the sector model for moderate and strong wind experiments ($\tau = 0.1$ N m^{-2} and $\tau = 0.2$ N m^{-2}, respectively) with respect to the model without wind-forcing. Increasing wind stress forcing leads to decreasing carbon concentration and inventory in the ventilated thermocline. Note that the deep ocean carbon concentration changes very little. (a) moderate—no wind, (b) strong—no wind.

wind stress of around 0.2 N m^{-2}, the sensitivity of atmospheric pCO_2 becomes weaker in the numerical experiments, suggesting a convergence with the idealized value of $\tau^{1/2}$.

c. Upper ocean control

Figure 10 illustrates the sensitivity of the oceanic reservoirs of carbon to changes in the Ekman pumping. With increasing wind stress, ventilated thermocline C decreases due to the shorter residence time of water parcels at the surface and increasing undersaturation at the point of subduction. In contrast there is very little change in the deep ocean C (Fig. 10). The upper ocean controls the sensitivity of pCO_2^{at} to wind-stress in strong contrast to the sensitivity to surface properties, such as temperature, which is controlled by the large deep ocean reservoir.

Why does the deep ocean carbon reservoir show such a small change in C? The deep waters do indeed become increasingly undersaturated as the wind-stress forcing increases since the shorter surface residence time also impacts the subpolar region (Fig. 11). In the deep ocean, however, the enhanced undersaturation, ΔC, is almost completely compensated by the increase in C_{eq}, the saturation C, due to the increase in pCO_2^{at}. Globally, changes in ocean C are buffered, stabilizing the ocean-atmosphere carbon partitioning—see, for example (Bolin and Eriksson, 1959).

A simple ocean and atmosphere box model illustrates the compensation of C_{eq} and ΔC which must hold for the global ocean. We define the global mean ocean C concentration $\bar{C} = (V_d C_d + V_{th} C_{th})/(V_d + V_{th})$ (see Fig. 3). From this and (1) we may relate $\bar{C}$ and pCO_2^{at} through mass balance. They must obey, $MpCO_2^{at} + V\bar{C} =$ constant, where M is the number of moles of gas in the atmosphere, and $V = V_d + V_{th}$ is the total volume of the ocean. Consider small perturbations in atmospheric pCO_2 and mean ocean C concentration.

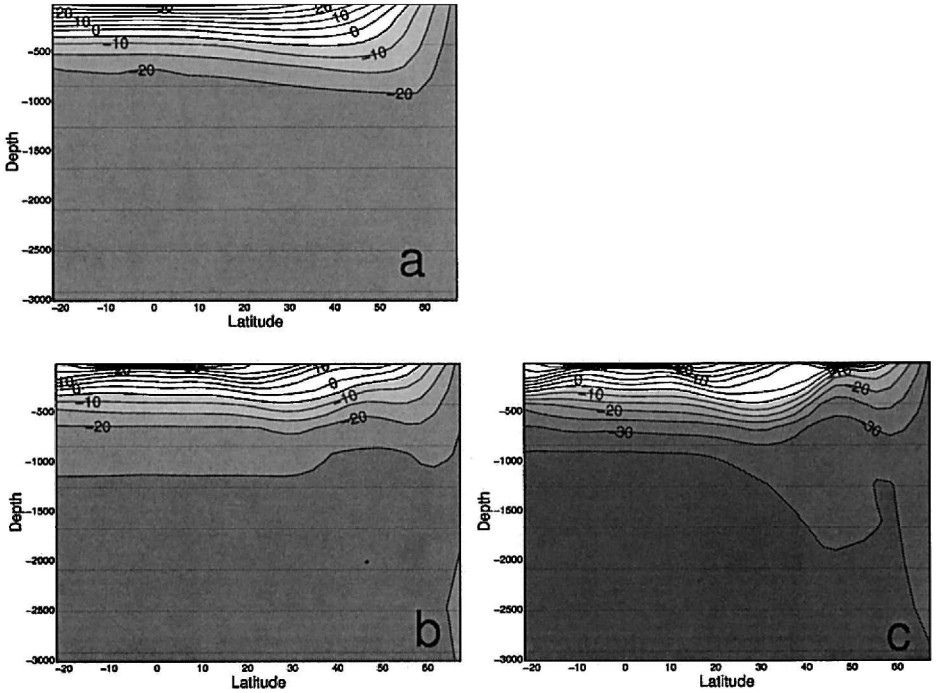

Figure 11. Zonally averaged saturation state, ΔC (μmol kg^{-1}), of the sector model for cases (a) without wind forcing, (b) moderate wind forcing, and (c) strong wind forcing. Both upper and deep ocean become increasingly undersaturated as wind stress increases due to the decreasing surface residence time which prevents full equilibration with the atmosphere. However, the undersaturation of the large deep ocean reservoir is largely compensated by buffering and the increase in the saturated concentration. Hence deep ocean C is stabilized and insensitive to changes in wind stress forcing (Fig. 10).

$$M\delta pCO_2^{at} + V\delta\bar{C} = 0. \tag{27}$$

Following (6), a perturbation in $\bar{C}$ must be the sum of perturbations in $\overline{C_{eq}}$ and $\overline{\Delta C}$ in the abiotic limit.

$$\delta\bar{C} = \delta\overline{C_{eq}} + \delta\overline{\Delta C}. \tag{28}$$

Combining (28) with the definition of the Revelle or buffer factor (Bolin and Eriksson, 1959), $(\delta pCO_2^{at}/pCO_2^{at})/(\delta C_{eq}/C_{eq}) = B_u \sim O(10)$ we find an expression for the change in global mean C:

$$\delta\bar{C} = \left(\frac{C_{eq}}{B_u pCO_2^{at}}\right)\delta pCO_2^{at} + \delta\Delta C. \tag{29}$$

Combining (29) with the linearized mass balance (27) we can evaluate the sensitivity of the ocean mean carbon concentration, $\bar{C}$, to the saturation state, $\overline{\Delta C}$:

$$\frac{\partial \overline{C}}{\partial \overline{\Delta C}} = \left(1 - \frac{1}{1 + \dfrac{MB_u p\mathrm{CO}_2^{at}}{V\overline{C_{eq}}}} \right) \sim 0.2. \tag{30}$$

This relationship tells us that, in the globally averaged, steady state, a change in saturation state, $\delta\overline{\Delta C}$, *must* be largely compensated by a corresponding change in the saturation carbon concentration, $\delta\overline{C_{eq}}$ due to increasing atmospheric $p\mathrm{CO}_2$. Hence the resulting change in $\overline{C}$ is moderate. $\overline{\delta C} \sim 0.2\delta\overline{\Delta C}$.

The effect of undersaturation due to intense surface currents is mediated by the compensating increase in C_{eq}. In the three-dimensional, sector ocean model we find a significant decrease in upper ocean C due to increased wind forcing. However, the global constraint, (30), is facilitated by compensation between C_{eq} and ΔC in the large deep ocean reservoir. It is the warm, upper ocean waters which dominate the sensitivity of atmospheric $p\mathrm{CO}_2$ to changes in wind-stress in contrast to the more widely considered sensitivity to changes in surface properties (e.g., temperature or alkalinity) which is controlled by the cold high latitudes and deep ocean reservoir.

d. Combined effects of wind and diapycnal mixing: Numerical experiments

Possibly in the ocean, and certainly in ocean circulation models, the thermocline structure is significantly influenced by both wind and diapycnal mixing. Using the numerical model, we map out the sensitivity of atmospheric $p\mathrm{CO}_2$ to the combined effects of diapycnal mixing and wind-stress forcing in the idealized, abiotic sector model (Fig. 12).

The effects of diapycnal diffusion and wind-driven circulation are competitive. When diapycnal diffusivity is large, atmospheric $p\mathrm{CO}_2$ is less sensitive to the variations in the wind stress forcing. In this case, the upper ocean is mainly dominated by the diffusive thermocline. In contrast, when diapycnal diffusivity is sufficiently small ($\kappa \sim 10^{-5}\,\mathrm{m^2\,s^{-1}}$), the ventilated thermocline and wind-stress forcing dominate the sensitivity of atmospheric $p\mathrm{CO}_2$. Scalings (23) and (26) are in excellent agreement with the numerical simulations in the limiting regimes. The idealized scalings discussed in the previous sections correspond to the axes of the plot in Figure 12.

In general, increasing either wind-stress amplitude or diapycnal mixing rates increases atmospheric CO_2 over most of the explored parameter space. In the case of diapycnal mixing, this is due to an increase in the volume of warm waters and a decrease in the mean ocean solubility of CO_2. In the case of wind forcing, it is due to the combination of the deepening of the ventilated thermocline and the increasing undersaturation of thermocline waters as the transit time through the western boundary current system becomes short relative to air-sea gas exchange times. These model results suggest that, over reasonable ranges of variability in these parameters, atmospheric $p\mathrm{CO}_2$ could vary by as much as 30 ppmv.

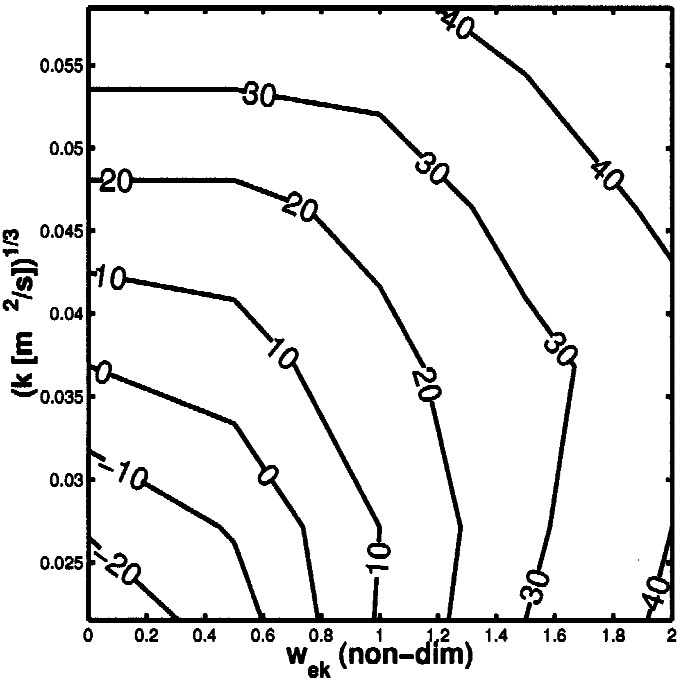

Figure 12. Steady state atmospheric pCO_2 as a function of diapycnal diffusivity and wind-stress forcing amplitude. Horizontal axis is the nondimensionalized Ekman pumping, and vertical axis is the ⅓ power of diapycnal diffusivity.

5. Summary and discussion

We have developed a general theory for the solubility pump of carbon in an abiotic ocean with a fixed alkalinity. For a closed ocean-atmosphere system, atmospheric pCO_2 varies inversely with the oceanic budget. The oceanic budget of carbon is controlled by the thermal structure of the ocean which largely dictates the effective carbon loading if all water masses were saturated at the point of subduction. This is modulated by the degree of saturation of the subducted waters. Hence, for this system, atmospheric pCO_2 varies with the product of thermocline thickness and thermocline dissolved inorganic carbon concentration.

For a simple, single-basin ocean, without wind forcing, the surface residence times are long and subducted waters are close to equilibrium with the overlying atmosphere. Hence pCO_2 varies with the volume of warm waters or thermocline thickness which, in this limit, scales with $\kappa^{1/3}$: the diapycnal mixing coefficient to the one third power. For an inviscid ocean with wind forcing the thickness of the subtropical thermocline scales as $w_{ek}^{1/2}$, the square root of the Ekman pumping rate. Surface ocean currents are swift, subduction occurs before waters have equilibrated with the overlying atmosphere and the ventilated thermocline is undersaturated. Over a wide range of Ekman pumping rates, the degree of undersaturation scales linearly with w_{ek}. Hence atmospheric pCO_2 varies as $w_{ek}^{2/3}$. Dissolved inorganic carbon in the ventilated thermocline, C_{th}, is reduced as the wind-stress

forcing (and undersaturation) increases. These scalings accurately predict the sensitivities of an ocean model of intermediate complexity: The MIT ocean model configured in a single hemisphere basin, with abiotic carbon cycle and a coupled atmospheric CO_2 reservoir.

In contrast to the response to other physical influences, the sensitivity to wind-stress changes is facilitated by the upper ocean, and not the large carbon reservoir of the deep oceans. Classical box models of the ocean carbon cycle infer a dominant role for the large, deep ocean reservoir and high latitude oceans in modulating the solubility pump, and thus atmospheric pCO_2. The sensitivity to surface properties, e.g. temperature and alkalinity, is controlled by the high latitudes through the deep ocean reservoir. The subtropical oceans and ventilated thermocline dominate the sensitivity of atmospheric pCO_2 to changes in surface wind-stress in abiotic carbon cycle models. The intense, wind-driven circulation strongly affects the saturation state of both upper oceans and abyss. Increasing wind-stress leads to increased undersaturation, a decreased ocean carbon budget, and an increase in atmospheric pCO_2. However, changes in atmospheric pCO_2, and equilibrium C, compensate those in the saturation state in the deep ocean. As a result, the deep ocean carbon loading is largely unchanged by the variations in the wind-stress. The change in atmospheric pCO_2 is attributable to changes in the subtropical, upper ocean saturation state and carbon budget.

The theory and models suggest a dominant and significant role for the upper ocean in modulating the response of atmospheric pCO_2 to changes in the wind stress forcing, as has occurred in past climate changes. Doubling the wind-stress leads to an increase in atmospheric pCO_2 of as much as 30 ppmv in this model. Interestingly, this infers a mechanism which would *increase* atmospheric CO_2 during glacial climates where hemispheric temperature gradients and mid-latitude westerlies would likely be increased.

This study used highly idealized models to better understand aspects of a very complex system. Some of the simplifying assumptions are significant and the subject of continuing study. Notably, here we have focused on the impact of changes in wind stress on the physical structure of the ocean. We have not discussed the sensitivity of the gas transfer coefficient in order to facilitate no-wind experiments and to focus on other aspects of the physical dependence. However, this is the subject of an ongoing study. Here we have focused on an abiotic ocean and neglected biological influences. Of course it is likely that the biological pumps are also sensitive to changes in wind stress forcing (Boyle, 1986; 1988) and diapycnal mixing. We expect that an approach based on the one used here will also provide insight into the biological pumps and particularly their response in the subtropical oceans, to changes in climate and physical forcing. One further limitation of this study is the focus on dynamics related to ocean basins. The important region of the Antarctic Circumpolar Current and the Southern Ocean are controlled by different, or modified dynamics. We are studying this regime separately, but ultimately a global synthesis must emerge.

Acknowledgments. TI is thankful to the Geophysical Fluid Dynamics Program at Woods Hole Oceanographic Institution since this work started during the GFD summer school in 2001. MJF is grateful for support from NSF (OCE-0136609). Two anonymous reviewers and R. Williams provided useful suggestions which improved the manuscript.

REFERENCES

Archer, D. E., A. Winguth, W. Broecker, R. Pierrehumbert, M. Tobis and R. Jacob. 2000. Atmospheric pCO_2 sensitivity to the biological pump in the ocean. Global Biogeochem. Cycles, *14,* 1219–1230.

Bacastow, R. B. 1995. The effect of temperature change of the warm surface waters of the oceans on atmospheric CO_2. Global Biogeochem. Cycles, *10,* 319–334.

Bolin, B. and E. Eriksson. 1959. Changes in the carbon dioxide content of the atmosphere and sea due to fossil fuel combustion, *in* Distribution of Matter in the Sea and Atmosphere, B. Bolin, ed., Rockefeller Inst. Press, NY, 130–142.

Boyle, E. A. 1986. Deep ocean circulation, preformed nutrients, and atmospheric carbon dioxide: Theories and evidence from oceanic sediments, *in* Mesozoic and Cenozoic Oceans, Geodynamics Series, *15,* AGU, 49–59.

——— 1988. The role of vertical chemical fractionation in controlling late Quaternary atmospheric carbon dioxide. J. Geophys. Res., *93,* 15701–15714.

Broecker, W. S. and T. H. Peng. 1974. Gas exchange rates between air and sea. Tellus, *26,* 21–35.

——— 1982. Tracers in the Sea, Eldigio Press, Lamont-Doherty Observatory of Columbia University, 1–689.

——— 1993. Greenhouse Puzzles, Eldigio Press, Lamont-Doherty Observatory of Columbia University, 1–251.

Broecker, W. S., J. Lynch-Stieglitz, D. Archer, M. Hoffmann, E. Maier-Reimer, O. Marchal, T. Stocker and N. Gruber. 1999. How strong is the Harvardton-Bear constraint? Global Biogeochem. Cycles, *13,* 817–820.

Bryan, F. 1987. Parameter sensitivity of primitive equation ocean general circulation models. J. Phys. Oceanogr., *17,* 970–985.

DOE. 1994. Handbook of Methods for the Analysis of the Various Parameters of the Carbon Dioxide System in Sea Water, Version 2, A. G. Dickson and C. Goyet, eds., ORNL/CDIAC-74, 1–22.

Follows, M. J., T. Ito and J. Marotzke. 2002. The wind-driven, subtropical gyres and the solubility pump of CO_2. Global Biogeochem. Cycles, *16,* 1113, doi:10.1029/2001GB001786.

Follows, M. J., R. G. Williams and J. C. Marshall. 1996. The solubility pump in the subtropical gyre of the North Atlantic. J. Mar. Res., *54,* 605–630.

Follows, M. J. and R. G. Williams. 2003. Mechanisms controlling the air-sea flux of CO_2 in the North Atlantic Ocean, *in* Ocean Carbon Cycle and Climate, T. Oguz and M. Follows, eds., NATO ASI volume (submitted).

Gent, P. R. and J. C. McWilliams. 1990. Isopycnal mixing in ocean circulation models. J. Phys. Oceanogr., *20,* 150–155.

Gnanadesikan, A. 1999. A simple, predictive model for the structure of the oceanic pycnocline. Science, *283,* 2077–2079.

Goyet, C. and A. Poisson. 1989. New determination of carbonic acid dissociation constants in sea water as a function of temperature and salinity. Deep-Sea Res., *36,* 1635–1654.

Gruber, N., J. L. Sarmiento and T. F. Stocker. 1996. An improved method for detecting anthropogenic CO_2 in the ocean. Global Biogeochem. Cycles, *10,* 809–837.

Iselin, C. O'D. 1939. The influence of vertical and lateral turbulence on the characteristics of waters at mid-depths. Trans. Amer. Geophys. Union, *20,* 414–417.

Knox, F. and M. B. McElroy. 1984. Changes in atmospheric CO_2: Influence of the marine biota at high latitude. J. Geophys. Res., *89,* 4629–4637.

Ledwell, J. R., A. J. Watson and C. S. Law. 1993. Evidence for slow mixing across the pycnocline from an open ocean tracer-release experiment. Nature, *364,* 231–246.

Luyten, J. R., J. Pedlosky and H. Stommel. 1983. The ventilation thermocline. J. Phys. Oceanogr., *13,* 292–309.

Marotzke, J. and J. R. Scott. 1999. Convective mixing and the thermohaline circulation. J. Phys. Oceanogr., *29,* 2962–2970.

Marshall, J. C., A. J. G. Nurser and R. G. Williams. 1993. Inferring the subduction rate and period over the North Atlantic. J. Phys. Oceanogr., *23,* 1315–1329.

Marshall *et al.* 1997a. Hydrostatic, quasi-hydrostatic, and non-hydrostatic ocean modeling. J. Geophys. Res., *102(C3),* 5733–5752.

Marshall *et al.* 1997b. A finite-volume, incompressible Navier Stokes model for studies of the ocean on parallel computers. J. Geophys. Res., *102(C3),* 5753–5766.

McKinley, G., M. Follows and J. C. Marshall. 2000. Interannual variability of the air-sea flux of oxygen in the North Atlantic. Geophys. Res. Lett., *27,* 2933–2936.

Park, Y. G. and K. Bryan. 2000. Comparison of thermally driven circulations from a depth-coordinate model and an isopycnal layer model, Part I. Scaling law sensitivity to vertical diffusivity. J. Phys. Oceanogr., *30,* 590–605.

Pedlosky, J. 1986. Thermocline theories, *in* General Circulation of the Ocean, H. G. I. Abardanel and W. R. Young, eds., Springer-Verlag, NY, 55–101.

——— 1996. Ocean Circulation Theory, Springer-Verlag, NY,

Roy, R. N., L. N. Roy, K. M. Vogel, C. Portermoore, T. Pearson, C. E. Good, F. J. Millero and D. M. Campbell. 1993. Determination of the ionization constants of carbonic acid in sea water in salinities 5 to 45 and temperatures 0 to 45°C. Mar. Chem., *44,* 245–267.

Samelson, R. and G. K. Vallis. 1997. Large-scale circulation with small diapycnal diffusivity: the two-thermocline limit. J. Mar. Res., *55,* 223–275.

Sarmiento, J. L. and J. R. Toggweiler. 1984. A new model for the role of the oceans in determining atmospheric pCO_2. Nature, *308,* 620–624.

Scott, J. R. 2000. The roles of mixing, geothermal heating, and surface buoyancy forcing in ocean meridional overturning dynamics, Ph.D. Thesis, Massachusetts Institute of Technology.

Siegenthaler, U. and T. Wenk. 1984. Rapid atmospheric CO_2 variations and ocean circulation. Nature, *308,* 624–626.

Sigman, D. M. and E. A. Boyle. 2000. Glacial-interglacial variations in atmospheric carbon dioxide. Nature, *407,* 819–928.

Stommel, H. 1979. Determination of watermass properties of water pumped down from the Ekman layer to the geostrophic flow below. Proc. Nat. Acad. Sci. U.S., *76,* 3051–3055.

Stumm, W. and J. J. Morgan. 1996. Aquatic Chemistry, 3rd Edition, John Wiley and Sons, NY, 1022 pp.

Takahashi, T., R. A. Feely, R. F. Weiss, R. H. Wanninkhof, D. W. Chipman, S. C. Sutherland and T. T. Takahashi. 1997. Global Air-Sea Flux of CO_2: An estimate based on measurements of sea-air pCO_2 difference. Proc. Nat. Acad. Sci., *94,* 8292–8299.

Toggweiler, J. R., A. Gnanadesikan, S. Carson, R. Murnane and J. L. Sarmiento. 2003. Representation of the carbon cycle in box models and GCMs: 1. Solubility pump. Global Biogeochem. Cycles, *17(1),* 1026, doi: 10.1029/2001GB001401.

Vallis, G. K. 2000. Large-scale circulation and production of stratification: Effects of wind, geometry, and diffusion. J. Phys. Oceanogr., *30,* 933–954.

Volk, T. and M. I. Hoffert. 1985. Ocean carbon pumps: analysis of relative strength and efficiencies in ocean driven atmospheric CO_2 changes, *in* The Carbon Cycle and Atmospheric CO_2: Natural Variations Archean to Present, E. T. Sandquist and W. S. Broecker, eds., AGU, Washington, D.C., 99–110.

Weiss, R. F. 1974. Carbon dioxide in water and sea water: The solubility of a non-ideal gas. Mar. Chem., *2,* 203–215.

Zhang, J., R. W. Schmitt and R. X. Huang. 1999. The relative influence of diapycnal mixing and hydrologic forcing on the stability of the thermohaline circulation. J. Phys. Oceanogr., *29,* 1096–1108.

Received: *4 February, 2003;* revised: *16 June, 2003.*